J|A|C|S ARTICLES

Published on Web 08/04/2009

The Molecular Mechanism of the Catalase Reaction

Mercedes Alfonso-Prieto,[†,‡] Xevi Biarnés,[†,#] Pietro Vidossich,[†,‡] and Carme Rovira*[,†,‡,§]

Laboratori de Simulació Computacional i Modelització (CoSMoLab), Parc Científic de Barcelona, Josep Samitier 1-5, 08028 Barcelona, Spain, Institut de Química Teòrica i Computacional (IQTCUB), and Institució Catalana de Recerca i Estudis Avançats (ICREA), Passeig Lluís Companys, 23, 08018 Barcelona, Spain

Received March 10, 2009; E-mail: crovira@pcb.ub.es

Abstract: Catalases are ubiquitous enzymes that prevent cell oxidative damage by degrading hydrogen peroxide to water and oxygen ($2H_2O_2 \rightarrow 2\ H_2O + O_2$) with high efficiency. The enzyme is first oxidized to a high-valent iron intermediate, known as Compound I (Cpd I) which, in contrast to other hydroperoxidases, is reduced back to the resting state by further reacting with H_2O_2. By means of hybrid QM/MM Car−Parrinello metadynamics simulations, we have investigated the mechanism of the reduction of Compound I by H_2O_2 in *Helicobacter pylori* catalase (HPC) and *Penicillium vitale* catalase (PVC). We found that the Cpd I−H_2O_2 complex evolves to a Cpd II-like species through the transfer of a hydrogen atom from the peroxide to the oxoferryl unit. To complete the reaction, two mechanisms may be operative: a *His-mediated* (Fita-Rossmann) mechanism, which involves the distal His as an acid−base catalyst mediating the transfer of a proton (associated with an electron transfer), and a *direct mechanism*, in which a hydrogen atom transfer occurs. Independently of the mechanism, the reaction proceeds by two one-electron transfers rather than one two-electron transfer, as has long been the lore. The calculations provide a detailed view of the atomic and electronic reorganizations during the reaction, and highlight the key role of the distal residues to assist the reaction. Additional calculations on the *in silico* HPC His56Gly mutant and gas-phase models provide clues to understand the requirements for the reaction to proceed with low barriers.

1. Introduction

Heme enzymes have long attracted biochemists for the wide range of chemical reactions they are able to catalyze. In cytochromes P450s, peroxidases and catalases, the active species responsible for oxidation and/or oxygenation reactions is a high-valent iron intermediate, known as Compound I (Cpd I),[1] obtained by reaction with hydrogen peroxide (H_2O_2, see reaction 1) and characterized to be an oxoferryl porphyrin cation radical ($Por^{\bullet+}-Fe^{IV}=O$) or an electromer of this.[1] The reactivity of Cpd I is determined by the protein frame in which the heme prosthetic group is buried and research aimed to grasp the origin of this functional diversity is an extremely active field.[2]

Heme catalases, present in almost all aerobically respiring organisms,[3−5] play an important role in defending cells against oxidative damage by degrading hydrogen peroxide (H_2O_2) to water and oxygen ($2H_2O_2 \rightarrow 2\ H_2O + O_2$). Catalases have been implicated as an important factor in inflammation,[6] mutagenesis,[7] prevention of apoptosis,[8] and stimulation of a wide spectrum of tumors.[9] Evidence from kinetics studies[3] indicate that once catalase Cpd I forms (reaction 1),[10] it rapidly reacts with a second molecule of H_2O_2 to generate O_2 and a water molecule (reaction 2).

$$\text{Enz (Por-Fe}^{III}\text{)} + H_2O_2 \rightarrow \text{Cpd I (Por}^{\bullet+}\text{-Fe}^{IV}\text{=O)} + H_2O \quad (1)$$

$$\text{Cpd I (Por}^{\bullet+}\text{-Fe}^{IV}\text{=O)} + H_2O_2 \rightarrow \text{Enz (Por-Fe}^{III}\text{)} + H_2O + O_2 \quad (2)$$

Reaction 2, extremely efficient in catalases, occurs at a much slower pace in a few other heme enzymes (e.g., chloroperoxidase

† Parc Científic de Barcelona (PCB).
‡ Institut de Química Teòrica i Computacional (IQTCUB).
# Current address: International School for Advanced Studies (SISSA/ISAS), Via Beirut 2-4, 34014 Trieste, Italy.
§ Institució Catalana de Recerca i Estudis Avançats (ICREA).

(1) Groves, J. T.; Haushalter, R. C.; Nakamura, M.; Nemo, T. E.; Evans, B. J. *J. Am. Chem. Soc.* **1981**, *103*, 2884–2886.
(2) See for instance: (a) Dawson, J. H. *Science* **1988**, *240*, 433–439. (b) *Handbook of Metalloproteins*; Messerschmidt, A., Huber, R., Poulos, T. L., Wieghardt, K., Eds.; John-Wiley and Sons: New York, 2001; Vol. 1. (c) Poulos, T. L. *Nat. Prod. Rep.* **2007**, *24*, 504–510. (d) de Visser, S. P.; Shaik, S.; Sharma, P. K.; Kumar, D.; Thiel, W. *J. Am. Chem. Soc.* **2003**, *125*, 15779–15788.
(3) Nichols, P.; Fita, I.; Loewen, P. C. Enzymology and structure of catalases. In *Advances in Inorganic Chemistry*; Sykes, A. G., Mauk, G., Eds.; Academic Press: New York, 2001; pp 51−106.
(4) Zámocký, M.; Koller, F. *Prog. Biophys. Mol. Biol.* **1999**, *72*, 19–66.
(5) Kirkman, H. N.; Gaetani, G. F. *Trends. Biochem. Sci.* **2007**, *32*, 44–50.
(6) Halliwell, B.; Gutteridge, J. M. C. *J. Biochem.* **1984**, *219*, 1–14.
(7) Vuillame, M. *Mutat. Res.* **1987**, *186*, 43–72.
(8) (a) Yabuki, M.; Kariya, S.; Ishisaka, R.; Yasuda, T.; Yoshioka, T.; Horton, A. A.; Utsumi, K. *Free Radical Biol. Med.* **1999**, *26*, 325–332. (b) Islam, K. N.; Kayanoki, Y.; Kaneto, H.; Suzuki, K.; Asahi, M.; Fuiji, J.; Taniguchi, N. *Free Radical Biol. Med.* **1997**, *22*, 1007–1017. (c) Sandstrom, P. A.; Buttke, T. M. *Proc. Natl Acad. Sci. U.S.A.* **1993**, *90*, 4708–4712.
(9) Miyamoto, T.; Hayashi, M.; Takeuchi, A.; Okamoto, T.; Kawashima, S.; Takii, T.; Hayashi, H.; Onozaki, K. *J. Biochem.* **1996**, *120*, 725–730.
(10) Jones, P.; Dunford, H. B. *J. Inorg. Biochem.* **2005**, *99*, 2292–2298.

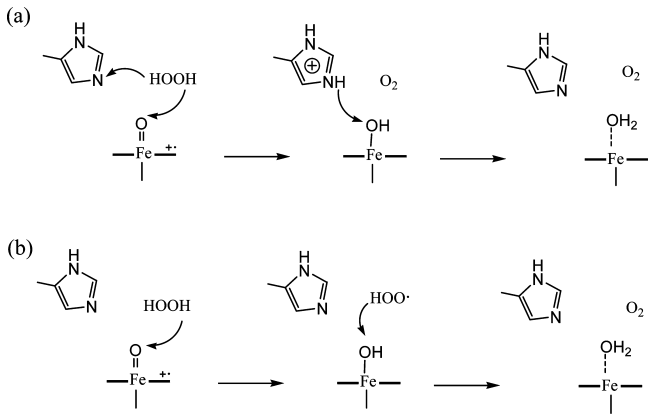

Figure 1. Proposed mechanisms of Cpd I reduction. (a) The *His-mediated* mechanism. (b) The *direct* mechanism.

(CPO), catalase-peroxidase (KatG) and myoglobin (Mb)).[11] The origin of this disparity has long been sought, and even though the catalase reaction has been known since 1940s,[3] the detailed mechanism of Cpd I reduction (reaction 2) has yet to be clarified. Reaction 2 is a two-electron redox process and clarifying whether it actually involves a two-electron transfer elementary step would pose catalases in clear contrast with peroxidases, for which the resting state is restored in two one-electron reduction processes.[10]

Isotope labeling kinetic studies on catalase early demonstrated that both oxygen atoms of the O_2 molecule originate from the same H_2O_2 molecule.[12] On the basis of the crystal structure of native bovine catalase, Fita and Rossmann proposed[13] that the two hydrogens of H_2O_2 are sequentially transferred to the oxoferryl unit of Cpd I, with the distal His playing an active role in the reaction. Recently, the group of Watanabe, by means of a detailed kinetic study, was able to disentangle the rate constants for reactions 1 and 2 for *Micrococcus lysodeikticus* catalase (MLC) and a series of myoglobin mutants.[14,15] Two different kinetic behaviors were observed in H_2O and D_2O for reaction 2, which were interpreted as two different mechanisms. Specifically, it was proposed that the reduction of Cpd I by H_2O_2 in native catalase, as well as in the F43H/H64L Mb mutant, follows the Fita-Rossmann model,[13] with the transfer of an hydride ion from H_2O_2 to the oxoferryl and the distal His acting as an acid−base catalyst to mediate the transfer of a proton (Figure 1a, hereafter named as the *His-mediated* mechanism). An alternative mechanism in which two hydrogen atoms of H_2O_2 are directly transferred to the oxoferryl group (Figure 1b), was proposed for certain Mb mutants lacking a distal residue that could act as acid−base catalyst (H64X; X being Ala, Ser and Asp, and L29H/H64L). It was also suggested that the space and polarity of the distal pocket are important factors for the accommodation of H_2O_2 at a suitable position for reaction.

Mutation of the distal His in catalases suppresses the ability to form Cpd I,[3] thus, making the experimental proof of the involvement of the His also in Cpd I reduction difficult. Molecular modeling may overcome this limitation easily, as the generation of the intermediate is not a limiting factor in an *in silico* experiment, and provided that the level of theory is adequate, modeling the reaction may bring useful insight into the atomic and electronic changes associated to it.

Density functional theory (DFT) and its extensions to account for protein and solvation effects (i.e., Quantum Mechanics/Molecular Mechanics (QM/MM) methods) have been applied with success to the study of heme proteins,[16] including the characterization of Cpd I of catalases,[17−20] peroxidases,[21−23] myoglobin,[24,25] catalase-peroxidase,[26] nitric oxide synthase,[27] cytochrome P450[2d,28,29] and the mechanism of its formation.[30] DFT has also been applied with success in the study of non-heme high-valent oxo-iron complexes.[31] To the best of our knowledge, the reduction mechanism of Cpd I by H_2O_2 has only been modeled in non-heme enzymes[32] and biomimetic molecules,[33,34] but not yet in heme catalase. We previously investigated the electronic configuration of catalase Cpd I[17] and the electronic state of the dioxygen molecule released in the catalase reaction.[35] On the basis of a qualitative analysis, we showed that the mode of electron transfer (ET) does not determine the spin state of the released oxygen, in contrast with previous proposals which assumed that hydride transfer would lead to singlet oxygen production.[36] In this work, we explicitly model

(11) Matsui, T.; Ozaki, S.; Liong, E.; Phillips, G. N., Jr.; Watanabe, Y. *J. Biol. Chem.* **1999**, *274*, 2838–2844.
(12) (a) Jarnagin, R. C.; Wang, J. H. *J. Am. Chem. Soc.* **1958**, *80*, 786–787. (b) Vlasits, J.; Jakopitsch, C.; Schwanninger, M.; Holubar, P.; Obinger, C. *FEBBS Lett.* **2007**, *581*, 320–324.
(13) Fita, I.; Rossmann, M. G. *J. Mol. Biol.* **1985**, *185*, 21–37.
(14) Kato, S.; Ueno, T.; Fukuzumi, S.; Watanabe, Y. *J. Biol. Chem.* **2004**, *279*, 52376–52381.
(15) Watanabe, Y.; Nakajima, H.; Ueno, T. *Acc. Chem. Res.* **2007**, *40*, 554–562.
(16) Bikiel, D. E.; Boechi, L.; Capece, L.; Crespo, A.; De Biase, P. M.; Di Lella, S; González Lebrero, M. C.; Martí, M. A.; Nadra, A. D.; Perissinotti, L. L.; Scherlis, D. A.; Estrin, D. A. *Phys. Chem. Chem. Phys.* **2006**, *8*, 5611–5628.
(17) (a) Alfonso-Prieto, M.; Borovik, A.; Carpena, X.; Murshudov, G.; Melik-Adamyan, W.; Fita, I.; Rovira, C.; Loewen, P. C. *J. Am. Chem. Soc.* **2007**, *129*, 4193–4205.
(18) (a) Wang, R.; de Visser, S. P. *J. Inorg. Biochem.* **2007**, *101*, 1464–1472. (b) de Visser, S. P. *Inorg. Chem.* **2006**, *45*, 9551–9557.
(19) Green, M. T. *J. Am. Chem. Soc.* **2001**, *123*, 9218–9219.
(20) Horner, O.; Oddou, J. L.; Mouesca, J. M.; Jouve, H. M. *J. Inorg. Biochem.* **2006**, *100*, 477–479. (d) Horner, O.; Mouesca, J. M.; Solari, P. L.; Orio, M.; Oddou, J. L.; Bonville, P.; Jouve, H. M. *J. Biol. Inorg. Chem.* **2007**, *12*, 509–525.
(21) Derat, E.; Cohen, S.; Shaik, S.; Altun, A.; Thiel, W. *J. Am. Chem. Soc.* **2005**, *127*, 13611–13621.
(22) (a) Bathelt, C. M.; Mulholland, A. J.; Harvey, J. N. *Dalton T.* **2005**, 3470–3476. (b) Harvey, J. N.; Bathelt, C. M.; Mulholland, A. J. *J. Comput. Chem.* **2006**, *27*, 1352–1362.
(23) Guallar, V. *J. Phys. Chem. B* **2008**, *112*, 13460–13464.
(24) Hersleth, H. P.; Ryde, U.; Rydberg, P.; Görbitz, C. H.; Andersson, K. K. *J. Inorg. Biochem.* **2006**, *100*, 460–476.
(25) Silaghi-Dumitriescu, R.; Reeder, B. J.; Nichols, P. *Biochem. J.* **2007**, *403*, 391–395.
(26) Vidossich, P.; Alfonso-Prieto, M.; Carpena, X.; Loewen, P. C.; Fita, I.; Rovira, C. *J. Am. Chem. Soc.* **2007**, *129*, 13436–13446.
(27) Cho, K. B.; Derat, E.; Shaik, S. *J. Am. Chem. Soc.* **2007**, *129*, 3182–3188.
(28) Guallar, V.; Friesner, R. A. *J. Am. Chem. Soc.* **2004**, *126*, 8501–8508.
(29) Altun, A.; Shaik, S.; Thiel, W. *J. Am. Chem. Soc.* **2007**, *129*, 8978–8987.
(30) (a) Derat, E.; Shaik, S. *J. Phys. Chem. B* **2006**, *110*, 10526–10533. (b) Derat, E.; Shaik, S.; Rovira, C.; Vidossich, P.; Alfonso-Prieto, M. *J. Am. Chem. Soc.* **2007**, *129*, 6346–637.
(31) See for instance: (a) Klinker, E. J.; Kaizer, J.; Brennessel, W. W.; Woodrum, N. L.; Cramer, C. J.; Que, L., Jr. *Angew. Chem., Int. Ed. Engl.* **2005**, *44*, 3690–3694. (b) Decker, A.; Rohde, J. U.; Klinker, E. J.; Wong, S. D.; Que, L, Jr.; Solomon, E. I. *J. Am. Chem. Soc.* **2007**, *129*, 15983–96. (c) Noack, H.; Siegbahn, P. E. *J. Biol. Inorg. Chem.* **2007**, *12*, 1151–62.
(32) Siegbahn, P. E. M. *Theor. Chem. Acc.* **2001**, *105*, 197–206.
(33) Abashkin, Y. G.; Burt, S. K. *Inorg. Chem.* **2005**, *44*, 1425–1432.
(34) (a) Wang, X.; Li, S.; Jiang, Y. *Inorg. Chem.* **2004**, *43*, 6479–6489. (b) Sicking, W.; Korth, H. G.; Jansen, G.; de Groot, H.; Sustmann, R. *Chemistry* **2007**, *13*, 4230–4245.
(35) Alfonso-Prieto, M.; Vidossich, P.; Rodríguez-Fortea, A.; Carpena, X.; Fita, I.; Loewen, P. C.; Rovira, C. *J. Phys. Chem. A* **2008**, *112*, 12842–12848.
(36) Jones, P.; Perkins, P. G. *Nature* **1967**, *215*, 129–132.

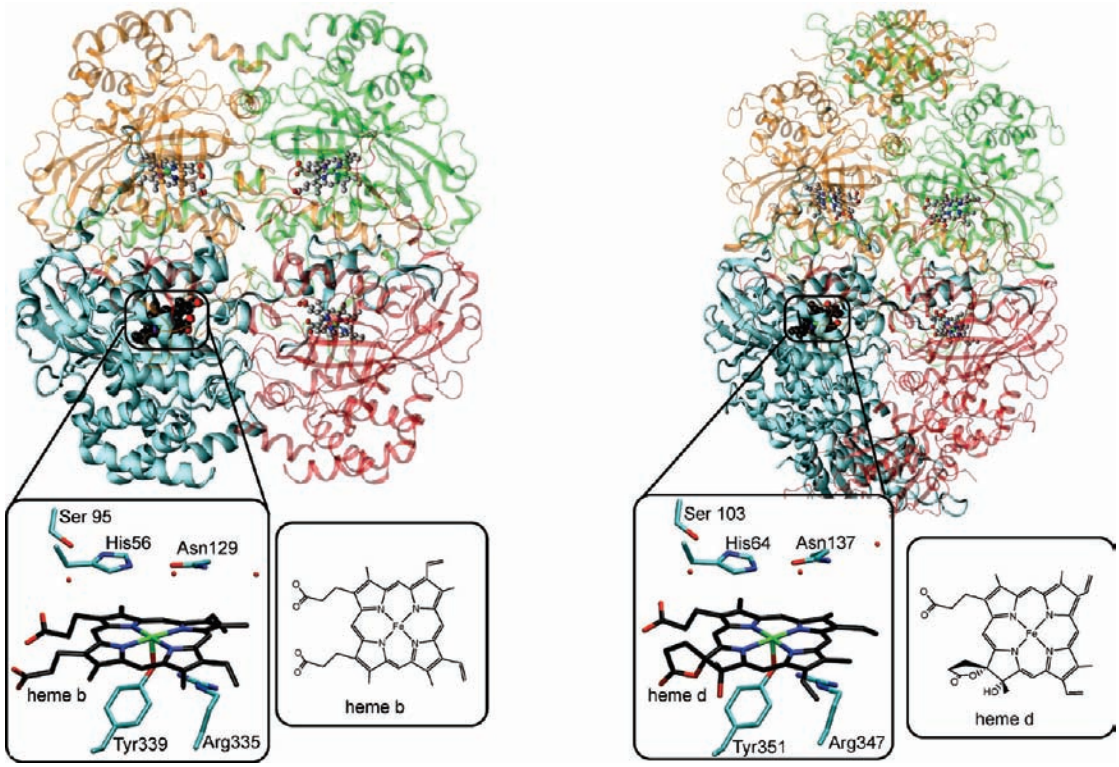

Figure 2. (a) Structure of native *H. pylori* catalase (HPC, PDB entry 2IQF). Top: cartoon picture of the protein, with the four subunits colored in blue, red, yellow and green, respectively. Bottom: heme binding pocket of one of the subunits (blue) and molecular structure of the heme b prosthetic group. (b) Same representation for *P. vitale* catalase (PVC, PDB entry 2IUF) and molecular structure of the heme d prosthetic group.

the mechanism of Cpd I reduction by H_2O_2 (reaction 2) by means of DFT QM/MM simulations. Our calculations are based on Car−Parrinello molecular dynamics (CPMD),[37] combined with the recently developed metadynamics approach,[38] which is aimed at enhancing the sampling of the reactive phase space and at mapping the underlying free energy landscape as a function of a small number of collective variables.

The calculations were performed on two different catalases: *Helicobacter pylori* catalase (HPC) and *Penicillium vitale* catalase (PVC), shown in Figure 2. The two proteins belong to different clades within the catalase family.[39] HPC is a small subunit clade 3 catalase, similar to other bacterial catalases such as *M. lysodeikticus* catalase (MLC) or *Proteus mirabilis* catalase (PMC) and contains heme b (iron protoporphyrin IX).[40] Instead, PVC is a large subunit clade 2 catalase and contains heme d (Figure 2b).[41,42] In heme d, one of the propionates has converted in a *cis*-hydroxy-γ-spirolactone and the corresponding pyrrole ring has lost the double-bond between the outer C_β carbon atoms. The calculations on both catalases allow testing the influence of the type of heme and the different protein environment on the molecular mechanism. In HPC, two alternative pathways were found that differ in the role of the distal His in the reaction. One pathway corresponds to the *His-mediated* (Fita-Rossmann)[13] mechanism (Figure 1a), with the distal His acting as an acid−base catalyst, while the other pathway represents the *direct* mechanism of Kato et al.[14] (Figure 1b), in which the distal His does not play an active role. Analysis of the atomic and electronic rearrangements show that, independently of the pathway, the reaction can be formally described by two one-electron transfers rather than one two-electron transfer, as it has been commonly assumed. In PVC, only the *His-mediated* mechanism was observed. Further calculations on the *in silico* HPC His56Gly mutant revealed that, when the acid−base catalyst is removed, the reaction may proceed only through the direct mechanism, with different energy barriers with respect to the wild-type enzyme. Additional DFT calculations on gas-phase models provided clues to rationalize these findings and to interpret the available experimental data.

2. Methods

2.1. Setup of the System. The initial structures for the QM/MM simulations were taken from our previous work,[17] based on the crystal structure of Cpd I of *H. pylori* catalase (HPC, PDB entry 2IQF, Figure 1a) and *P. vitale* catalase (PVC, PDB entry 2IUF). The details of the classical MD simulations performed to equilibrate each structure are given in the Supporting Information (SI, pages S2−S3). Once the system was equilibrated, QM/MM simulations were initiated. To model the Cpd I−H_2O_2 complex, the H_2O_2 molecule was accommodated into the active site as proposed by Fita and Rossmann.[13] The following QM-MM partition was used.

(37) (a) Car, R.; Parrinello, M. *Phys. Rev. Lett.* **1985**, *55*, 2471–2474. (b) Marx, D.; Hutter, J.; Ab initio molecular dynamics: Theory and implementation. In *Modern Methods and Algorithms of Quantum Chemistry*; Grotendorst, J., Ed.; John von Neumann Institute for Computing: Julich, Germany, 2000; pp 301−409. (c) CPMD program, Copyright IBM Corp. 1990−2003, Copyright MPI für Festkörperforschung, Stuttgart 1997−2001. URL: http://www.cpmd.org.
(38) (a) Laio, A.; Parrinello, M. *Proc. Nat. Acad. Sci. U.S.A.* **2002**, *99*, 12562–12566. (b) Iannuzzi, M.; Laio, A.; Parrinello, M. *Phys. Rev. Lett.* **2003**, *90*, 238302(4).
(39) Chelikani, P.; Fita, I.; Loewen, P. C. *Cell. Mol. Life Sci.* **2004**, *61*, 192–208.
(40) Loewen, P. C.; Carpena, X.; Rovira, C.; Ivancich, A.; Perez-Luque, R.; Haas, R.; Odenbreit, S.; Nicholls, P.; Fita, I. *Biochemistry* **2004**, *43*, 3089–3103.
(41) Vainshtein, B. K.; Melik-Adamyan, W. R.; Barynin, V. V.; Vagin, A. A.; Grebenko, A. I. *Nature (London, U.K.)* **1981**, *293*, 411–412.
(42) Díaz, A.; Valdés, V.-J.; Rudiño-Piñera, E.; Horjales, E.; Hansberg, W. *J. Mol. Biol.* **2009**, *386*, 218–232.

The QM region included the iron-porphyrin with its methyl and vinyl groups, the *p*-methylphenolate side chain of the proximal Tyr339/351 (residue numbering of HPC/PVC),[17] and the methylguanidinium side chain of Arg335/347, which is hydrogen bonded to the phenolate oxygen atom of Tyr339/351. Previous work demonstrated that both Tyr and Arg proximal residues influence significantly the structure and ligand properties of the heme.[43] The *cis*-hydroxy-γ-spirolactone modification present in heme d (Figure 2b) was fully included in the QM region. On the distal side of the heme, the side chains of residues Asn129/137, His56/64, Ser95/103 (which interacts with His56/64), hydrogen peroxide and two additional water molecules (hydrogen bonded to the distal residues Asn129/137 and Ser95/103 and conserved in X-ray structures)[2b,3] were also included in the QM region. The MM region comprised the rest of the model. Because of the enormous size of the protein, the calculations were performed on a reduced model consisting of all residues within 20 Å from the heme iron. This corresponds to a sizable protein fragment (4141 and 4986 atoms, respectively, in HPC and PVC) and it is expected to account for all the relevant heme−protein interactions affecting the electronic structure at the active center. Except for the presence of the hydrogen peroxide molecule, this is the same setup that we used in our previous work on catalase Cpd I.[17]

2.2. QM/MM Simulations. The QM/MM method developed by Laio, VandeVondele and Röthlisberger[44] combining the first principles molecular dynamics method of Car and Parrinello (CPMD)[37] with a force-field molecular dynamics methodology (i.e., QM/MM CPMD) was used. The general details of this method can be found in the SI (page S3). Previous work has demonstrated the reliability of this method in the description of structural, energetic and dynamic properties of systems of biological interest, including hemeproteins[17,26,45,46] The calculations were made using the generalized gradient-corrected approximation of the spin-dependent density functional theory (DFT-LSD), following the prescription of Becke and Perdew[47] and a plane wave basis set up to a kinetic energy cutoff of 70 Ry. *Ab initio* pseudopotentials, generated within the Troullier-Martins scheme,[48] were used. In the case of iron, an eight valence electrons supplemented with nonlinear core corrections (NLCC)[49] was employed. The QM system was enclosed in an isolated supercell of size $15.341 \times 21.160 \times 21.160$ Å^3 (HPC and $22.483 \times 18.780 \times 18.515$ Å^3 (PVC). Structure optimizations were performed by means of molecular dynamics with annealing of the atomic velocities, until the maximum component of the nuclear gradient was lower than 10^{-4} au. A similar setup was used in our previous works on heme proteins.[17,26,43,50] CP QM/MM simulations at an average temperature of 300 K were performed (2 ps) in order to equilibrate the system before starting the metadynamics simulations. A time step of 0.12 fs and a fictitious electronic mass of the CP Lagrangian of 700 au were used. The AMBER force field[51] was used to account for interactions among the atoms of the MM region.

Single-point calculations with other exchange correlation functionals (B3LYP[52] and PBE[53]), using the same PW basis set,[54] were perfomed to assess the error in relative energies of the local minima due to the functional employed. The energy difference between two stationary points (B1 and Cpd II-like, see Results) changed by +0.21/−2.6 kcal/mol with PBE/B3LYP. Thus, we estimate an upper bound of 2.6 kcal/mol for the dependence of the relative energies on the functional employed.

2.3. QM Calculations on Model Systems. The dependence of the energy barrier for hydrogen abstraction on the donor−acceptor distance was investigated using a reduced model consisting of the bare porphyrin with no substituents, the peroxide and the proximal tyrosinate (modeled as phenolate) together with the interacting arginine (modeled as methyl guanidinium). For fixed oxoferryl-peroxide distances ($d(O-O_{a/b}) = 2.5, 3.0, 3.5$ Å) the energetics for the transfer of H_a (or H_b) was calculated, optimizing all other degrees of freedom. Details of the DFT calculations are as for the QM/MM simulations described above.

GGA functionals, like the Becke-Perdew one used in this work, usually underestimate energy barriers of hydrogen abstraction reactions and may result in a poor description of open-shell species due to the self-interaction error.[55,56] To assess the accuracy of the Becke-Perdew functional in describing reactive oxygen species, we compared optimized gas phase geometries to experimental data of $HO_2^{\bullet}$ ($S = 1/2$), O_2^- ($S = 1/2$) and O_2 ($S = 1$), which show a good agreement (Table S1). We also computed the spin density of each molecule in a box of water molecules (see Figure S1). It turned out that the integrated spin densities are $HO_2^{\bullet}$, 0.97; O_2^-, 0.97; O_2, 1.95. Therefore, the Becke-Perdew calculations of the peroxyl radical, superoxide and dioxygen do not suffer of the severe spin delocalization as it occurs, for example, for the hydroxyl radical ($HO^{\bullet}$, $S = 1/2$), for which the integrated spin density is 0.69.[57] In addition, we computed the energy barrier for the first hydrogen atom abstraction (transfer of H_a to the oxoferryl oxygen) with a hybrid functional (B3LYP), which is known to be less affected by the self-interaction error than the Becke-Perdew functional (see section 3.4.1).[55]

2.4. Metadynamics Simulations. Metadynamics (MTD)[38] is a novel molecular dynamics based technique aimed at enhancing the sampling of the phase space and at estimating the free energy landscape. The general details of this method are described in the SI (pages S3−S4). An extended Lagrangian version of the method is here used for a proper coupling with the QM/MM simulations.[38b] Values of 3 (m_1) and 30 (m_2) amu for the mass of the fictitious particle and 3 (k_1) and 30 (k_2) au for the force constant were used in the MTD simulations (the subindexes 1 and 2 refer to the two collective variables, described below). The height of the Gaussian terms was set at 1 kcal·mol^{-1}, which ensures sufficient accuracy for the reconstruction of the free energy surface.[58] The width of the Gaussian terms was set at 0.03 according to the oscillations of the selected collective variables (see below) observed in a free dynamics. A new Gaussian-like potential was added every 150 MD

(43) Rovira, C.; Fita, I. *J. Phys. Chem. B* **2003**, *107*, 5300–5305.
(44) Laio, A.; vandeVondele, J.; Röthlisberger, U. *J. Chem. Phys.* **2002**, *116*, 6941–6947.
(45) See for instance: (a) Carloni, P.; Röthlisberger, U.; Parrinello, M. *Acc. Chem. Res.* **2002**, *35*, 455–464. (b) Dal Peraro, M.; Ruggerone, P.; Raugei, S.; Gervasio, F. L.; Carloni, P. *Curr. Opin. Struct. Biol.* **2007**, *17*, 149–156.
(46) Dal Peraro, M.; Spiegel, K.; Lamoureux, G.; De Vivo, M.; DeGrado, M.; Klein, M. L. *J. Struct. Biol.* **2007**, *157*, 444–453.
(47) (a) Becke, A. D. *J. Chem. Phys.* **1986**, *84*, 4524–4529. (b) Perdew, J. P. *Phys. Rev. B.* **1986**, *33*, 8822–8824.
(48) Troullier, M.; Martins, J. L. *Phys. Rev. B* **1991**, *43*, 1993–2006.
(49) Louie, S. G.; Froyen, S.; Cohen, M. L. *Phys. Rev. B* **1982**, *26*, 1738–1742.
(50) (a) Rovira, C.; Kunc, K.; Hutter, J.; Ballone, P.; Parrinello, M. *J. Phys. Chem. A* **1997**, *101*, 8914–8925. (b) Rovira, C.; Parrinello, M. *Chem.−Eur. J.* **1999**, *5*, 250–262. (c) Rovira, C.; Parrinello, M. *Biophys. J.* **2000**, *78*, 93–100. (d) Rovira, C.; Schulze, B.; Eichinger, M.; Evanseck, J. D.; Parrinello, M *Biophys. J.* **2001**, *81*, 435–445.
(51) Pearlman, D. A.; Case, D. A.; Caldwell, J. W.; Ross, W. S.; Cheatham, T. E.; Debolt, S.; Ferguson, D.; Seibel, G.; Kollman, P. *Comput. Phys. Commun.* **1995**, *91*, 1–41.
(52) (a) Becke, A. D. *Phys. Rev. A* **1988**, *36*, 3098–3100. (b) Lee, C.; Yang, W.; Parr, R. G. *Phys. Rev. B* **1988**, *37*, 785–789. (c) Becke, A. D. *J. Chem. Phys.* **1993**, *98*, 5648–5652.
(53) Perdew, J. P.; Burke, K.; Ernzerhof, M. *Phys. Rev. Lett.* **1996**, *77*, 3865−3868. Erratum: *Phys. Rev. Lett.* **1997** *78*, 1396.
(54) Todorova, T.; Seitsonen, A. P.; Hutter, J.; Kuo, I-F. W.; Mundy, C. *J. Phys. Chem. B.* **2006**, *110*, 3685–3691.
(55) (a) Perdew, J. P.; Staroverov, V. N.; Tao, J.; Scuseria, G. E. *Phys. Rev. A* **2008**, *78*, 052513. (b) Pu, J.; Truhlar, D. G. *J. Phys. Chem. A* **2005**, *109*, 773−778. (c) Aguilera-Iparaguirre, J.; Curran, H. J.; Klopper, W.; Simmie, J. M. *J. Phys. Chem. A* **2008**, *112*, 7047–7054.
(56) Blumberger, J. *Phys. Chem. Chem. Phys.* **2008**, *10*, 5651–5667.
(57) VandeVondele, J.; Sprik, M. *Phys. Chem. Chem. Phys.* **2005**, *7*, 1363–1367.

steps. To completely explore the free energy landscape, it was necessary to add 349/306 Gaussians for HPC/PVC. In terms of simulation time, this corresponds to $5.3 \times 10^4/4.2 \times 10^4$ MD steps (6.4/5.1 ps). Additional calculations working selectively in one of the two pathways found for HPC were done to probe the convergence of the FES. The height of the energy barrier changed within 1 kcal/mol, which corresponds to the resolution of the hills being used. In the case of PVC, the back reaction (from products to reactants) occurred while the product oxygen molecule was escaping toward the main channel. All our attempts to avoid it, by using either constraints or walls in the metadynamics simulation, did not succeed. Therefore, the free energy landscape will be represented using only the forward reaction.

The collective variables used in the metadynamics simulation were taken as a combination of coordination indices of the covalent bonds being formed/broken. Specifically, the first collective variable was taken as the coordination number between the two oxygen atoms of the H_2O_2 molecule and their two hydrogens, $CV_1 = N_{coord}$ (O_a, O_b; H_a, H_b) (i.e., A = O_a, O_b; B = H_a, H_b formula S1 (see SI for the definition of of N_{coord}).[59] An interesting feature of CV_1 is that it does not dictate which hydrogen is bonded to which oxygen during the simulation (i.e., H_b-O_b, H_a−O_a, H_b−O_a or H_a−O_b), but each hydrogen is allowed to coordinate to any oxygen (i.e., the two hydrogen atoms and the two oxygen atoms of H_2O_2 are treated in an equivalent way). The second collective variable was taken as the coordination number between the oxoferryl oxygen and the two peroxide hydrogens $CV_2 = N_{coord}$ (O; H_a, H_b) (i.e., A = O; B = H_a, H_b in formula S1).

The values of the two collective variables at the initial (CV_1, $CV_2 \approx 0.5, 1.0$) and final states (CV_1, $CV_2 \approx 0.0, 2.0$) of the process are different enough to ensure that the two states will appear in different regions of the free energy surface, a necessary condition for a suitable characterization of the reaction path in a metadynamics simulation.[58] It is important to note that this choice of the collective variables does not force nor restrict that any of the two peroxide hydrogens bind to the distal His during the reaction. Exploratory calculations using a single reaction coordinate failed to describe correctly the reaction under investigation (pages S6−S9 of the SI).

The ground state of catalase Cpd I is a quartet (S = 3/2), which also turned out to be the ground state of the Cpd I−H_2O_2 complex. For products, either quartet or octet are expected as ground states based on the spin state of the isolated fragments (triplet dioxygen; sextet Fe^{III}) and depending on whether spins couple ferro- or antiferromagnetically. Thus, we decided to run the metadynamics on the quartet state and investigate this single surface approximation a posteriori, computing the relative energies among different spin states (doublet, quartet, sextet and octet) for the main reaction intermediates (see Results).

3. Results

3.1. The Reactants (Cpd I−H_2O_2 Complex). As initial guess for the orientation of hydrogen peroxide in the active site of catalase Cpd I, we used the conformation proposed by Fita and Rossmann,[13] in which H_2O_2 forms hydrogen bonds with the distal His and Asn residues, as well as with the oxoferryl unit. These initial structures were optimized without any constraint for both the HPC and PVC complexes. In the optimized geometries (Figure 3a,b), the H_2O_2 molecule accommodates into the distal pocket maintaining the initial H-bond pattern. The H-bonds formed with the distal His and the oxoferryl oxygen are rather short (1.64/1.56 Å, respectively, for HPC and 1.66/1.72 Å for PVC), whereas the one formed with the NH_2 group of the distal Asn residue is presumably weaker (2.26 Å in HPC and 2.28 Å in PVC).

To explore other possible orientations of the H_2O_2 molecule, 2 ps *ab initio* molecular dynamics (CPMD) simulation were performed. For HPC, during the simulation, transfer of one hydrogen atom from the H_2O_2 molecule to the oxoferryl unit was observed, resulting in a complex between a hydroxoferryl species and a peroxyl radical (HOO•). In the final structure (Figure 3c), the peroxyl radical is hydrogen bonded to the distal His (His-N_ε···H_b-OO = 1.51 Å) and to the hydroxoferryl unit (HO-O···H_aO−Fe = 1.86 Å), keeping the weak hydrogen bond with the distal Asn (2.47 Å). The peroxyl radical is characterized by a reduction of the O−O distance (1.31 Å) with respect to the H_2O_2 molecule in the Cpd I−H_2O_2 complex (1.47 Å) and a spin density distribution originating from the unpaired electron in a π orbital (i.e., the molecular orbital formed by the two p_π oxygen orbitals, see Figure S2 of the SI). In addition, the iron−oxygen distance increases from 1.70 to 1.76 Å and the porphyrin cation radical of Cpd I is quenched. The spin density distribution of the hydroxoferryl heme (Figure S2) resembles that of catalase Cpd II: a triplet state with two unpaired electrons on the hydroxoferryl unit.[17,60] Therefore, H_a transfers as a hydrogen atom.

For PVC, the CP QM/MM dynamics led to different results. As in HPC, H_a is transferred from the peroxide to the oxoferryl unit (Figure 3d). However, the second hydrogen of H_2O_2 (H_b) was also transferred, as a proton, to the distal His. The resulting state is a Cpd II-like species and a superoxide ion, with the distal His protonated (Cpd II···O_2^-···$HisH^+$) (Figure 3d). In both cases (HPC and PVC), to reach the products state, it is still necessary for the second hydrogen atom of hydrogen peroxide (H_b) to "travel" to the hydroxoferryl oxygen.

3.2. Reaction Free Energy Landscape. Metadynamics simulations for both HPC and PVC started from the Cpd II-like configurations, which formed spontaneously during the initial room temperature equilibrium CP QM/MM simulations (Figure 3c,d). The evolution of the system during the metadynamics simulation is described in the SI (pages S10−S17, Figures S5−S12). We here report the free energy landscapes that were reconstructed from the simulations.

To better understand the free energy landscapes, let us note the physical meaning of the two collective variables. The first collective variable [$CV_1 = N_{coord}$ (O_a, O_b; H_a, H_b)] gives an idea of the degree of detachment of the two hydrogens from the two hydrogen peroxide oxygens. At the beginning of the simulation (Figure 3c,d), only one hydrogen is coordinated to a peroxide oxygen (O_b−H_b), thus, $CV_1 \approx 0.5$ (see formula S1; note that, because $N_A = 2$, a factor 1/2 applies). At the end of the simulation, none of the peroxide hydrogens are bonded to either O_a or O_b, thus, $CV_1 \approx 0$. The second collective variable [$CV_2 = N_{coord}$ (O; H_a, H_b)] indicates the degree of formation of the product water molecule. At the beginning of the simulation (Figure 3c,d), one hydrogen atom is coordinated to the ferryl oxygen (O−H_a), thus, $CV_2 \approx 1.0$, according to formula S1 (note that, in this case, $N_A = 1$, thus, no prefactor applies in the

(58) (a) Ensing, B.; De Vivo, M.; Liu, Z. W.; Moore, P.; Klein, M. L. *Acc. Chem. Res.* **2006**, *39*, 73–81. (b) Ensing, B.; Laio, A.; Parrinello, M.; Klein, M. L. *J. Phys. Chem.* **2005**, *109*, 6676–6687. (c) Laio, A.; Rodriguez-Fortea, A.; Gervasio, F. L.; Ceccarelli, M.; Parrinello, M. *J. Phys. Chem. B* **2005**, *109*, 6714–6721.

(59) The use of the coordination index of the bond being broken [$CV_1 = N_{coord}$ (O_b, H_b)] and the other one corresponding to the bond being formed [$CV_2 = N_{coord}$ (O, H_b)] is not a good idea since the free energy map (associated to the metadynamics simulation) would not allow to differentiate among all states of the reaction, which would appear very close in the free energy surface.

(60) Rovira, C. *ChemPhysChem* **2005**, *6*, 1–8.

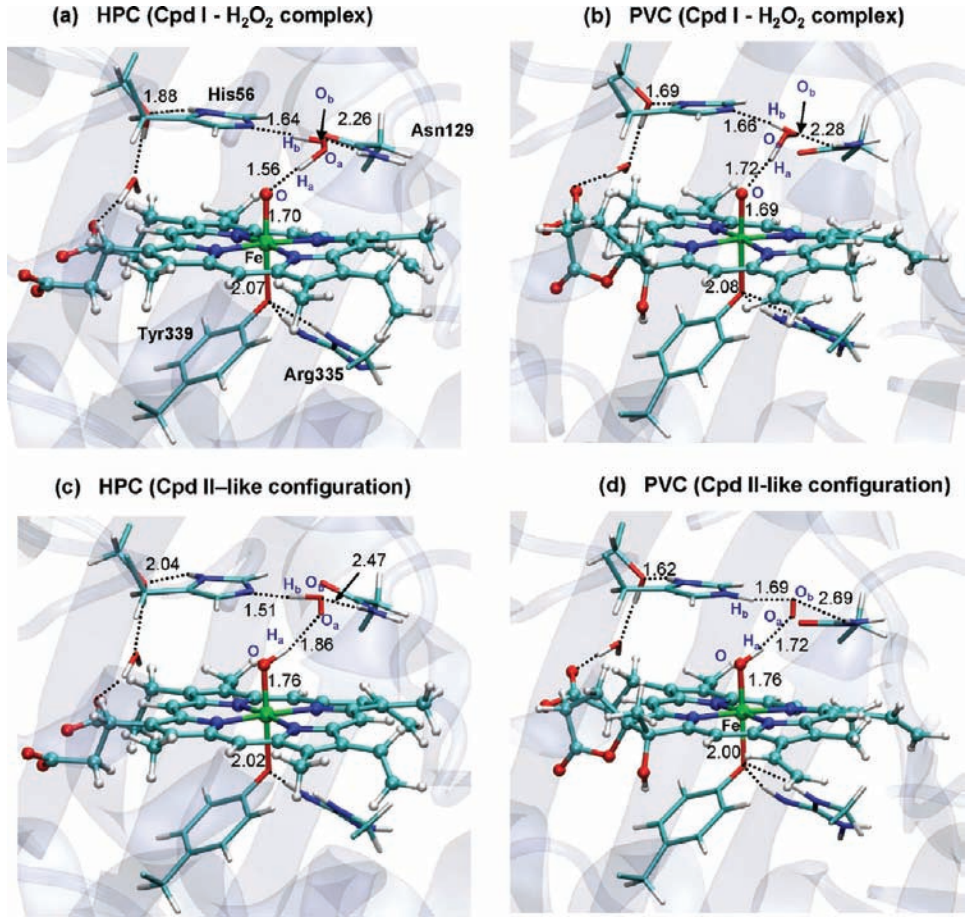

Figure 3. (a) Optimized structure of the HPC-Cpd I$-H_2O_2$ complex. The intramolecular distances of the H_2O_2 molecule are $H_a-O_a = 1.04$ Å, $H_b-O_b = 1.05$ Å, $O_a-O_b = 1.47$ Å. (b) Optimized structure of the PVC-Cpd I$-H_2O_2$ complex: $H_a-O_a = 1.01$ Å, $H_b-O_b = 1.03$ Å, $O_a-O_b = 1.51$ Å. (c) Average structure of the Cpd II-like species obtained after CP QM/MM simulation of (a): $H_a-O_a = 0.99$ Å, $O_a-O_b= 1.31$ Å, $O-H_b = 1.08$ Å. (d) Average structure of the Cpd II-like species obtained after CP QM/MM simulation of (b): $H_a-O_a = 1.00$ Å, $O_a-O_b= 1.27$ Å, $N_\varepsilon-H_b = 1.05$ Å.

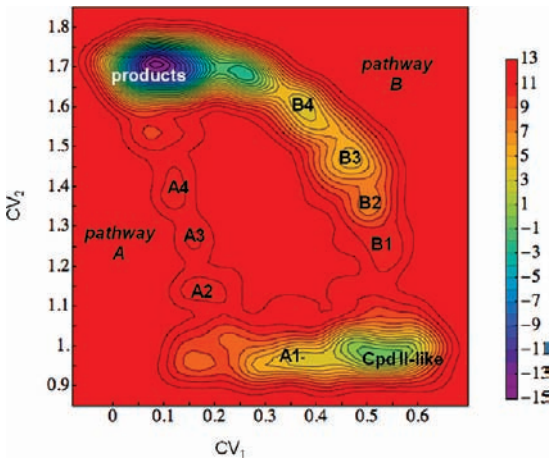

Figure 4. Free energy landscape reconstructed from the metadynamics simulation of HPC. Energies are in kilocalories per mole (kcal/mol).

formula). At the end of the simulation, the two peroxide hydrogens are bonded to O, thus, $CV_2 \approx 2$.

3.2.1. HPC. The free energy surface (FES) reconstructed from the metadynamics simulation of HPC is shown as a contour plot in Figure 4. Two competing pathways joining the Cpd II-like$-$HOO• complex and products valleys appear clearly differentiated. Each pathway contains several local minima of different well depth, separated by transition states. The atomic and spin reorganization along pathway **A** is shown in Figure 5. Following proton transfer (PT) to the distal His, the $HisH^+-O_2^-$ complex is formed (basin A1 in Figure 4 and representative snapshot shown in Figure 5). Afterward, the distal His rotates such that it breaks the H-bond with the superoxide anion (A2, Figures 4 and 5). At the same time, the hydroxoferryl group rotates with respect to the Fe$-$O bond, breaking the hydrogen bond with O_2^-, and positioning one oxygen lone pair in a suitable orientation to interact with the histidine proton (A3). A4 differs from A3 in the degree of rotation of the distal His around the $C_\beta-C_\gamma$ bond and the absence of hydrogen bond between the hydroxoferryl hydrogen and O_2^-. In the products state, H_b has been transferred to the hydroxoferryl oxygen, the Fe$-$O distance has increased (from 1.83 ± 0.06 Å in A4 to 2.08 ± 0.07 Å in the products), and a water molecule has been formed. The decrease of the O$-$O distance (from 1.33 ± 0.02 Å in A1 to 1.25 ± 0.02 Å in the products, see Table 1), together with the change of the spin density distribution (Figure 5 and Table 1), signals the change from O_2^- to O_2. Altogether, *pathway A consists of an electron transfer from O_2 to reduce Fe(IV) to Fe(III) early in the path, followed by a proton transfer from the distal His to Fe$-$OH.* Interestingly, the distal Asn changes conformation gradually (from the Cpd II-like configuration to the products), allowing the release of the product oxygen toward the main channel. Structures A2, A3, and A4 are at similar energies, 8 kcal/mol over A1 (Figure 4). Thus, the transition state along this pathway would correspond to all the process

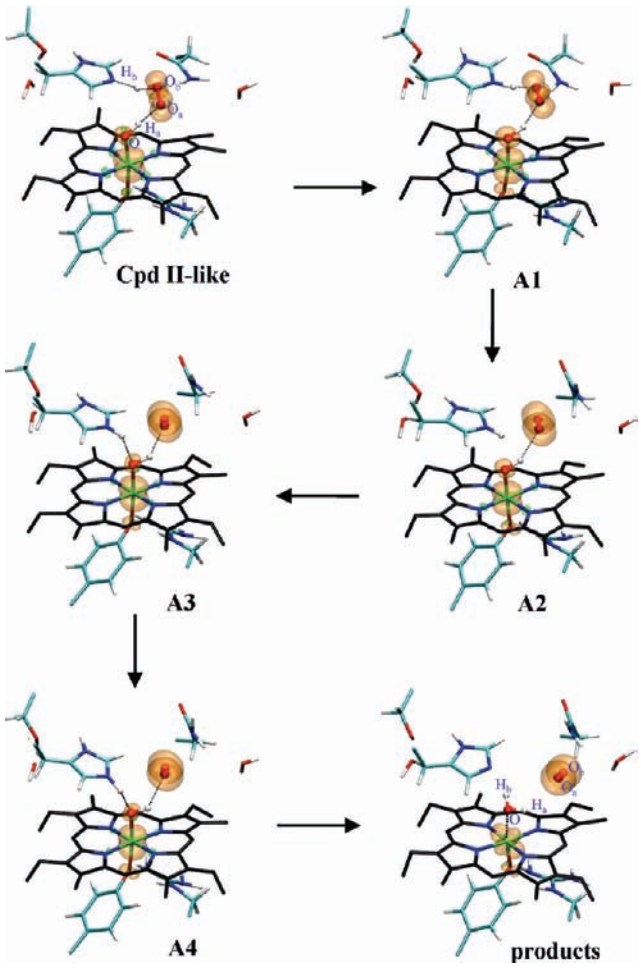

Figure 5. Atomic rearrangement along reaction pathway **A** in HPC. Spin isodensity surfaces at 0.007 e Å^{-3} are plotted in orange.

Table 1. Distances and Number of Unpaired Electrons of Relevant Fragments for Stationary Points along Pathways **A** and **B** of HPC[a]

	distance (Å)		number of unpaired electrons[61]			
structure	O−H_b	O_a−O_b	Fe=O	O_a−O_b	Porph	Tyr
Cpd I−H_2O_2	(3.19)	(1.47)	2.15	0.23	0.52	0.06
Cpd II-like	(3.68)	(1.34)	1.87	0.99	0.10	0.02
	3.45 ± 0.23	1.35 ± 0.03				
A1	3.51 ± 0.13	1.33 ± 0.02	1.83	1.05	0.03	0.07
A2	2.41 ± 0.10	1.29 ± 0.02	1.65	1.45	0.01	0.07
A3	2.01 ± 0.06	1.28 ± 0.01	1.56	1.54	0.02	0.06
A4	1.73 ± 0.02	1.27 ± 0.02	1.52	1.65	0.01	0.10
B1	2.08 ± 0.08	1.34 ± 0.02	1.83	0.98	0.08	0.09
B2	1.79 ± 0.04	1.32 ± 0.00	1.72	1.00	0.22	0.03
B3	1.53 ± 0.05	1.33 ± 0.03	1.79	1.01	0.12	0.04
B4	1.29 ± 0.05	1.33 ± 0.03	1.66	1.07	0.22	0.01
Products	(1.02)	(1.25)	1.12	1.77	0.02	0.06
	1.01 ± 0.04	1.25 ± 0.02				

[a] Distances are given as averages along the metadynamics simulation, except for values in parentheses that refer to optimized structures. Spin densities correspond to representative snapshots along the path.

through A2, A3, and A4, that is, rupture of the H-bond between the superoxide and the distal $HisH^+$, rotation of the latter to form an H-bond with the hydroxoferryl and transfer of H_b toward it. The highest states along this sequence of events are 9 kcal/mol over A1 and 12 kcal/mol over the initial Cpd II-like state.

Representative structures corresponding to pathway **B** are shown in Figure 6. Along this path, the hydroxoferryl unit first rotates around the Fe−O bond, breaking the hydrogen bond with O_a (B1). Afterward, the peroxyl radical flips orientation with H_b changing hydrogen bond partner from the distal His to the hydroxoferryl oxygen (B2). The distal His, not involved in any hydrogen bond interaction, moves upward (B1 → B2) to facilitate the rotation of the peroxyl radical. Structures B2, B3, and B4 mainly differ for the O···H_b distance and the degree of rotation of the hydroxoferryl unit. Finally, transfer of H_b to the hydroxoferryl oxygen leads to the product water and oxygen molecules. The change in O−O distances (Table 1) from B4 (1.33 ± 0.03 Å) to the products (1.25 ± 0.02 Å), together with the changes in spin density distribution (Figure 6), evidences that H_b transfers as a hydrogen atom.

Once the oxygen molecule forms, the distal Asn rotates to facilitate its escape toward the main channel, as it was also observed for pathway **A**. This illustrates the interplay of the His and Asn active site residues in the catalytic mechanism and underlines the importance of taking into account their dynamics on the modeling of the reaction. Along pathway **B**, the highest barrier that the system needs to overcome is in going from the Cpd II-like intermediate to the B1 basin (12 kcal/mol), corresponding to the rupture of the H-bond between the hydroxoferryl and the peroxyl radical. From B1 onward, the energetic profile is downhill, with each intermediate lower in energy than the preceding one.

3.2.2. PVC. The reconstructed FES obtained from the metadynamics simulation of PVC is shown in Figure 7. Here, a

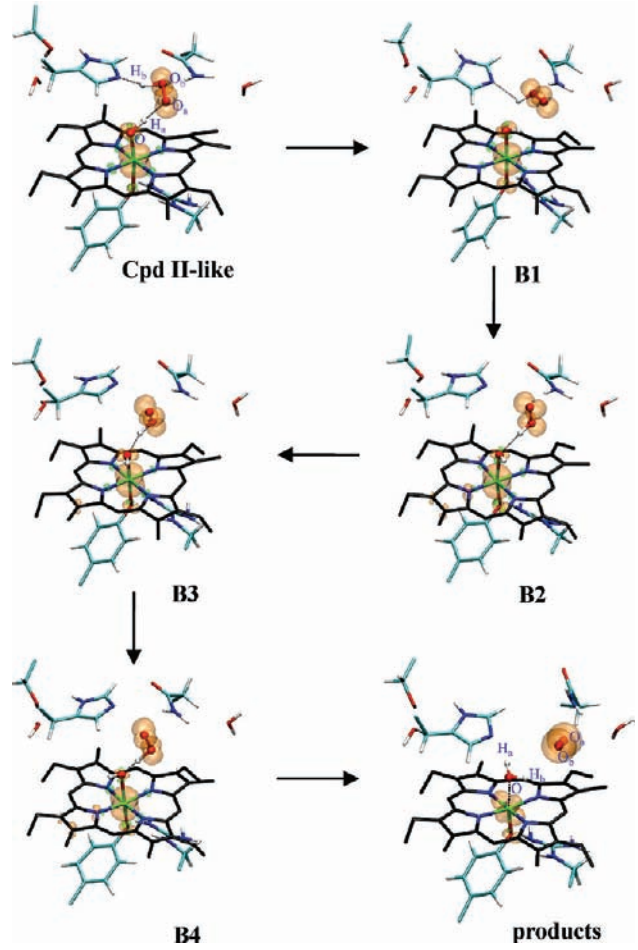

Figure 6. Atomic rearrangement along reaction pathway **B** in HPC. Spin isodensity surfaces at 0.007 e Å^{-3} are plotted in orange.

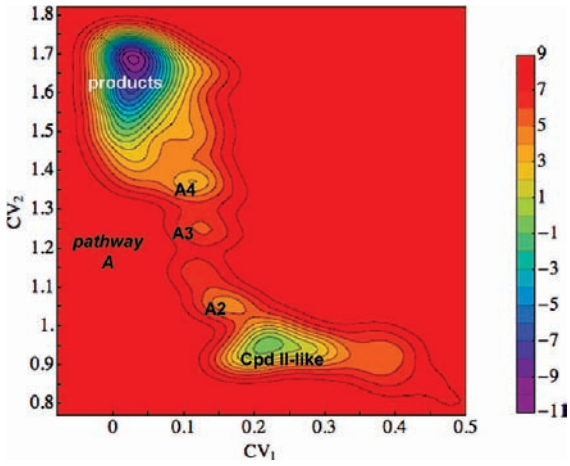

Figure 7. Free energy landscape reconstructed from the metadynamics simulation of PVC. Energies are given in kilocalories per mole (kcal/mol).

unique pathway joining the Cpd II-like$-O_2^{-}\cdots HisH^{+}$ species with the products valleys is found. Representative structures along this pathway are shown in Figure S13. Consistent with the finding that the PVC-Cpd I$-H_2O_2$ complex evolved spontaneously toward the Cpd II-like$-O_2^{-}\cdots HisH^{+}$ configuration during a room temperature CPMD simulation (Figure 3d), the FES shows only one minimum corresponding to this state ($CV_1 \sim 0.22$) and there is no minimum corresponding to $HO_2^{\bullet}\cdots$His (Figure 7). From the Cpd II-like$-O_2^{-}\cdots HisH^{+}$ configuration, the pathway involves the same intermediates as pathway **A** in HPC (hereafter, we name these two pathways as $\mathbf{A}^{HPC}$ and $\mathbf{A}^{PVC}$), that is, rotation of the distal His around $C_\beta-C_\gamma$ ($A2^{PVC}$, Figure S13), rotation of the hydroxoferryl group ($A3^{PVC}$ and $A4^{PVC}$, Figure S13) and subsequent transfer of H_b to the hydroxoferryl oxygen to form the products (Figure S13). The energy barrier along the pathway is similar to the one found in HPC for the corresponding steps (8 kcal/mol), with the highest energy state found in going from $A2^{PVC}$ to $A3^{PVC}$. However, considering that in HPC H_b has first to be transferred to the distal His, requiring 4 kcal/mol, path A^{PVC} results in 4 kcal/mol lower in free energy than A^{HPC}. The reason that $\mathbf{B}^{PVC}$ is not sampled in the metadynamics simulation could be due to the fact that it is higher in energy compared with pathway $\mathbf{A}^{PVC}$. However, the absence of minimum involving the peroxyl radical (the His$\cdots$HOO$^{\bullet}$ configuration is not stable in PVC) is probably the reason of the disappearance of pathway **B** in PVC.

3.2.3. Spin State Analysis. As described in section 2.4, the metadynamics simulations were constrained to the quartet spin state, which is the ground state of both Cpd I and the Cpd I$-H_2O_2$ complex (Table S3). To investigate this single surface approximation, we optimized the structure of the main reaction intermediates (the Cpd I$-H_2O_2$ complex, the Cpd II-like configuration and the products) in different spin states (doublet, quartet, sextet and octuplet) (Table S3). For the shallow minima along the reaction pathways (A1−A4 and B1−B4), no geometry optimization was attempted and only the vertical energy gap is given in Table S3. For all spin states, the released oxygen molecule is (locally) in a triplet state with two unpaired electrons (Table S4), as we found for catalase gas phase models.[35] The doublet and the quartet states were found to be very close in energy along the reaction, and thus, it is reasonable that at room temperature both species may coexist in equilibrium. The optimized structures of the Cpd I$-H_2O_2$ complex, the Cpd II-like configuration and the products in both spin states are nearly identical (see Table S4 and the simple picture on Figure S14), suggesting that there is no significant difference between the doublet and the quartet reaction surfaces, as already found for a nonheme catalase mimic.[34b] The sextet state was found to be the ground state of the products. This electronic configuration results from two unpaired electrons on dioxygen and three on Fe(III) (see simple picture on Figure S14). Even though the spin state of the products is not known experimentally, it would be expected that the local spin at the heme is the same as in the resting enzyme, that is, a high spin iron (sextet state).[62] Two possible explanations may account for this discrepancy. First, the prediction of an intermediate spin electronic configuration as the ground state of Fe(III) is a well-known deficiency of GGA functionals.[63,64] Alternatively, it could be that the spin state changes when O_2 is still in the heme pocket. In the optimized structure of the products in the sextet spin state, the iron−water distance is 3.29 Å, whereas in the X-ray structure of the native enzyme, this distance is longer (4.10−4.22 Å). Most likely, the exit of the oxygen molecule from the active site may increase the available space in the pocket and allow the water molecule to become hydrogen bonded to the distal His and Asn, as in the crystal structure. This further increase in the iron−water distance would result in a smaller splitting of the d-orbitals of the iron and a larger stabilization of the high-spin iron.

Table S3 shows that geometry relaxation greatly stabilizes the energy of the products in this spin state. A similar stabilization would bring configurations A1−A4 and B1−B4 closer to the sextet surface. However, we expect such geometry relaxation to be smaller in configurations A1−A4 and B1−B4 than in the products for the following reason. The products correspond to a configuration in which Fe(IV) has been reduced to Fe(III) and the axial hydroxyl is protonated (to form H_2O). These two conditions, which should result in a high spin 5-coordinated iron, as experimentally observed for the resting enzyme, are not given simultaneously in any of configurations A1−A4 and B1−B4. Although the electron transfer occurs early in pathway **A** (from A1 to A2), the proton passes to the hydroxyl only in the last step from A4 to products. Similarly, along pathway **B**, the hydrogen atom is transferred from B4 to the products. Thus, we infer that spin crossing (from quartet to sextet) would affect only the final step, formation of products. The octet state lies rather high in energy along the paths and is still higher than the quartet after geometry relaxation (reactants and products configurations). Thus, it is unlikely that it participates in the reaction. The amount of spin contamination, computed for the quartet state according to Wang et al.,[63] turns out to be small (<10% for optimized geometries and <15% for single points, Table S3). Thus, we conclude that the quartet free energy surface is representative of the process investigated.

3.3. Influence of the Distal His in Cpd I Reduction. Pathways $\mathbf{A}^{HPC}$ and $\mathbf{A}^{PVC}$, described above, point to the role of the distal histidine as an acid−base catalyst, facilitating the transfer of a proton from superoxide to the hydroxoferryl moiety. Site-directed mutation of the distal His in catalases suppresses the ability to form Cpd I, thus, making the experimental proof of the involvement of the His also in Cpd I reduction impossible. On the contrary, the role of His can be easily proved by molecular modeling. With this aim, we performed a CP QM/

(61) The spin density was integrated using Bader's Atoms-In-Molecules theory (Bader, R. F. W. Atoms in Molecules: A Quantum Theory; Oxford University Press: New York, 1990).
(62) Sharma, K. D.; Andersson, L. A.; Loehr, T. M.; Terner, J.; Goff, H. M. *J. Biol. Chem.* **1989**, *264*, 12772–12779.
(63) Ghosh, A. *J. Biol. Inorg. Chem.* **2006**, *11*, 712–724.
(64) Schöneboom, J. C.; Thiel, W. *J. Phys. Chem. B* **2004**, *108*, 7468–7478.

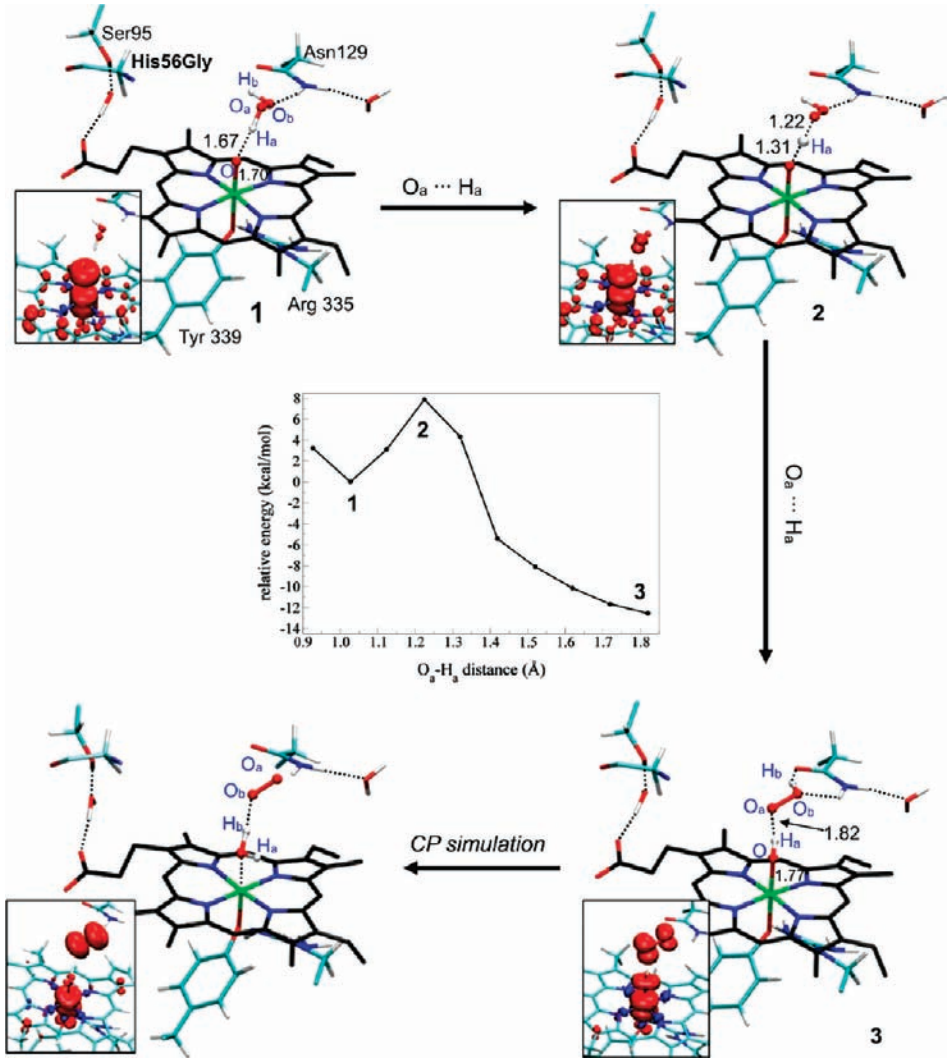

Figure 8. Energy profile for the stretching of the O_a-H_a distance in the His56Gly *in silico* mutant of HPC. The pictures represent three points (1, 2, 3) along the reaction coordinate. The spin density distribution is represented in the insets.

MM simulation of the HPC-Cpd I$-H_2O_2$ complex in the absence of the distal His side chain. This was accomplished by including His56 in the MM region and zeroing the charges and vdW parameters of its side chain (i.e., we generated an *in silico* His56Gly mutant). Starting from the same initial structure of the Michaelis complex as for the wild-type enzyme (described above), CP QM/MM simulations show that, contrary to native HPC, the transfer of one hydrogen atom from the H_2O_2 to the Fe═O unit is not spontaneous. Instead, a barrier of 8 kcal/mol was obtained by computing the potential energy profile along the $O_a\cdots H_a$ coordinate (Figure 8).

Contrary to what was observed in the wild-type enzyme, the second part of the reaction (from the Cpd II-like species to the products) took place spontaneously via pathway **B** (Figure 8). Therefore, the shape of the free energy landscape along mechanism **B** is drastically affected by the absence of the distal His.

3.4. Gas-Phase Model Calculations. To further investigate the effect of the distal His in Cpd I reduction, we performed gas-phase calculations on a simplified model without distal residues. We examined the dependence of the donor−acceptor distance on the energy barrier for the sequential transfer of H_a and H_b to the oxoferryl unit (steps 1 and 2, Figure 9).

3.4.1. Por$^{+\bullet}$-Fe(IV)O$-H_2O_2$ Complex. The potential energy profiles for the transfer of H_a from H_2O_2 to the oxoferryl oxygen (step 1) at various fixed oxygen−oxygen distances are shown in Figure 9 (top). The process is exothermic, with H_a transferred formally as a hydrogen atom (H•). The species formed are $HO_2^\bullet$ and Cpd II; thus, the porphyrin radical has been quenched. As H_a is transferred, the Fe−O distance lengthens, whereas O_a-O_b shortens. The barrier for the transfer shows a marked dependence on the $O_a\cdots$O(Fe) distance, being smaller for shorter interoxygen distances. For very short $O_a\cdots O$ distances (2.5 Å), the process is almost barrierless. The energy barriers computed with the B3LYP functional reproduce this tendency (Table S5), although the hybrid functional predicts a 4 kcal/mol barrier at short interoxygen distance.

3.4.2. Por-Fe(IV)OH$-HO_2^\bullet$ Complex. The energy profiles for the transfer of H_b from $HO_2^\bullet$ to the hydroxoferryl unit (step 2) at various fixed oxygen−oxygen distances are shown in Figure 9 (bottom). Like H_a, H_b transfers formally as a hydrogen atom, generating triplet dioxygen and low spin iron(III) coordinated to a water molecule. As the transfer proceeds, the Fe−O distance lengthens, whereas O_a-O_b shortens. Again, the barrier decreases for small interoxygen distances, the transfer being barrierless for a very short H-bond. These results will be discussed later on, in relation with the reaction mechanism in the absence of the distal His.

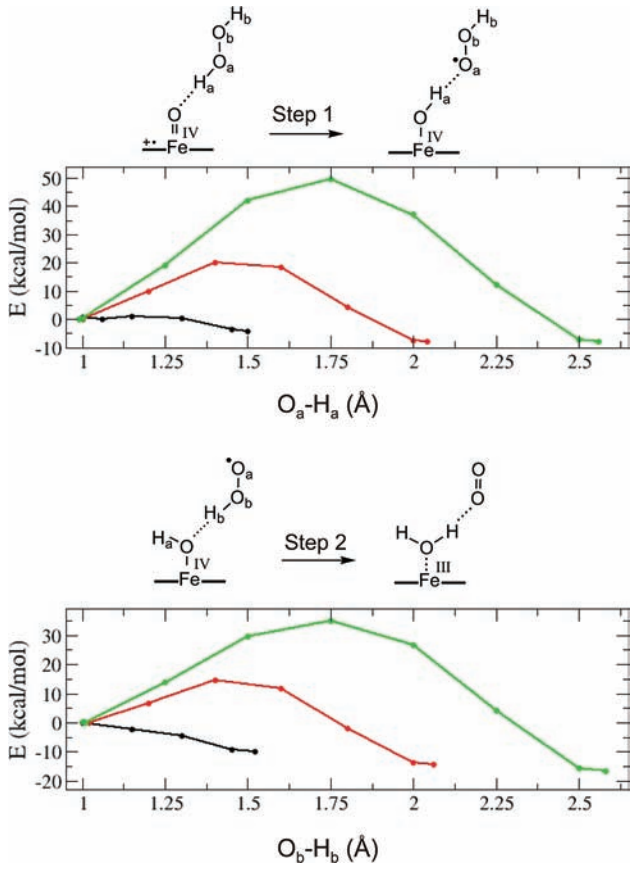

Figure 9. Energy profile for the transfer of H_a (Step 1, top) and H_b (Step 2, bottom) in a gas-phase catalase model, for various $O_{Fe}\cdots O_{a/b}$ distances: $d(O-O_{a/b}) = 2.5$ (black), 3.0 (red), 3.5 Å (green).

4. Discussion

Even though the catalase reaction has been known since the 1940s,[3] the mechanism of Cpd I reduction in catalase has not yet been modeled by quantitative (i.e., first-principles) approaches. This is attempted in this work by means of state-of-the-art QM/MM Car−Parrinello molecular dynamics simulations in *H. pylori* catalase (HPC) and *P. vitale* catalase (PVC). We have focused on the process that goes from the inner-sphere enzyme(Cpd I)−H_2O_2 complex to the products, without investigating the diffusion of H_2O_2 through the protein channel that leads to the active center. Mutagenesis studies showed that the size of the access channel may affect the efficiency of the catalase reaction.[3]

Our calculations show that the Enzyme(Cpd I)−H_2O_2 complex, both in HPC and PVC, evolves spontaneously at room temperature to a Cpd II-like species (Figure 3), in which formally a hydrogen atom transfer has occurred (proton transfer to the oxoferryl oxygen and electron transfer quenching the porphyrin radical of Cpd I). HPC and PVC differ in that in PVC the second proton of hydrogen peroxide is transferred too (to the distal His, forming $HisH^+\cdots O_2^-$, Figure 3d), whereas it is not in HPC ($His\cdots HO_2^\bullet$, Figure 3c). This difference may be understood considering that the intrinsic pK_a of a histidine (6.5, but proposed to be 5.0 in peroxidase Cpd I[10]) and that of $HO_2^\bullet$ (4.8)[65] are similar, and thus, slight changes in the environment may stabilize either of the two states ($HisH^+\cdots O_2^-$ or $His\cdots HO_2^\bullet$). HPC and PVC belong to different clades of the catalase family and share 47%/64% sequence identity/similarity (70%/77% considering residues within 10 Å from the Fe atom).[66] Attempts to calculate the pK_a of the distal His in Cpds I and II for the two proteins by solution of the Poisson−Boltzmann equation (data not shown) did not reproduce the above findings, possibly due to the limitations of the method used. A further difference between PVC and HPC is the nature of the prosthetic group: heme b in HPC, heme d in PVC. In heme d, a propionate formed a lactone with the porphyrin ring, resulting in a reduced overall charge (carboxylate to ester) of the active site and a 2-electron less porphyrin π system (one of the porphyrin double bonds is missing with respect to heme b). It could be argued that the different charge distribution between the two types of heme favors one state over the other. However, previous calculations of the HPC-Cpd I−H_2O_2 complex using a gas-phase model also converged to the $HisH^+\cdots O_2^-$ configuration.[35] Thus, we conclude that the protein frame is responsible for the stabilization of either $HisH^+\cdots O_2^-$ or $His\cdots HO_2^\bullet$ forms, although we could not identify the residues responsible of such effect.

Metadynamics simulations were used to investigate how the reaction proceeds from the Cpd II-like intermediate to the products. Two general collective variables (or reaction coordinates) that characterize the nuclear reorganization from reactants (oxoferryl + H_2O_2) to products (H_2O and O_2), without any preconceived assumption on the involvement of active site residues, were used to drive the reaction and reconstruct the free energy surface (FES). We found that HPC and PVC display a similar reaction pathway, corresponding to the *His-mediated* (Fita-Rossmann) mechanism, in which the distal His acts as an acid−base catalyst (A^{HPC} in Figure 6 and A^{PVC} in Figure S13). The free energy along this path shows a different profile in the two proteins (Figures 4 and 7), because, as explained above, the initial states are different ($HisH^+\cdots O_2^-$ in PVC, $His\cdots HO_2^\bullet$ in HPC), requiring the proton to be first transferred to the His in HPC. Once the $HisH^+\cdots O_2^-$ state is reached, the highest energy barriers are similar in the two proteins (9 kcal/mol in HPC and 8 kcal/mol in PVC) and correspond to the conformational change of the $HisH^+$ leading to the formation of an H-bond with the hydroxoferryl. Subsequently, the $HisH^+$ proton and one electron from O_2^- transfer to the hydroxoferryl unit. Besides the motion of the distal His, an interesting feature of the mechanism is the rotation of the distal Asn side chain toward the main channel (Figure 5), facilitating the escape of the oxygen molecule released in the reaction and supporting the previously proposed role of this residue in ligand entry/escape.[60,67] As discussed earlier, this could explain why the protein is engineered such that there is no hydrogen-bonding interaction toward the carbonyl oxygen atom of the distal Asn.[60,67] Such interactions would restrain its conformational flexibility and Asn would not be efficient for catalysis.

In HPC, a further pathway was observed (**B**, Figures 4 and 6), not involving residues of the active site. Mechanism **B** consists of the flip of $HO_2^\bullet$, with a barrier of 12 kcal/mol (Figure 4), and the subsequent transfer of a hydrogen atom ($H^\bullet$, Figure 6 and Table 1). Pathway B^{HPC}, together with the initial H transfer from H_2O_2 to the oxoferryl (Figure 3), is essentially the *direct mechanism* proposed by Kato et al. for certain myoglobin mutants.

(65) Hoare, J. P. In *Standard Potentials in Aqueous Solution*; Bard, A. J., Parsons, R., Jordan, J., Eds.; Marcel Dekker: New York, 1985, Ch. 4.
(66) Analysis excluding the variable N-terminal end and the C-terminal domain, following reference 42.
(67) Rovira, C.; Alfonso-Prieto, M.; Biarnés, X.; Carpena, X.; Fita, I.; Loewen, P. C. *Chem. Phys.* **2006**, *323*, 129–137.
(68) Bishop, G. R.; Davidson, V. L. *Biochemistry* **1995**, *34*, 12082–12086.
(69) (a) Jones; Perkins, *Nature* **1967**, *215*, 129–132. (b) Jones; Sugget, *Biochem. J.* **1968**, *110*, 621–629. (c) Dounce, *Theor. Biol.* **1983**, *105*, 553–567.

It is important to note that, due to the limitations of the method used (DFT with a pure GGA functional) in describing hydrogen abstraction processes, the energy barriers that we compute are approximate. In particular, it is expected that the conversion of the Cpd I−H_2O_2 complex to the Cpd II-like species, which occurs spontaneously in our calculations, has an energy barrier. Test calculations using a hybrid functional reproduce the variation of the energy barrier with interoxygen distance found in the GGA calculations, showing that, for short interoxygen distances, the barrier is small. This is consistent with the known ability of the Fe(IV)═O moiety to abstract hydrogen atoms. Therefore, our calculations capture the main features of the catalase reaction.

It is interesting to relate the computed mechanism with the results of previous experimental investigations. In their study, Kato et al. measured the kinetic isotope effect (KIE) in H_2O and D_2O for MLC and five Mb mutants. MLC belongs to the same clade classification as HPC, sharing 45%/66% sequence identity/similarity with HPC, and their active sites are identical. It is thus expected that they share a common mechanism. The myoglobin mutants in ref 14 were designed to probe the role of distal site residues in heme catalysis. Specifically, all the investigated mutants lack Mb-His64 which was shown to inhibit Cpd I formation. F43H/H64L and L29H/H64L were designed to investigate how the location of the distal His affects the catalase activity,[11] whereas H64A, H64S and H64D probed the effect of accessible volume and polarity of the distal pocket. Small KIE (< 4) were measured for MLC and the F43H/H64L mutant of Mb. The free energy landscape computed from metadynamics simulations shows that the most relevant barrier does not correspond to any H transfer in neither of the two highlighted pathways (**A** and **B**), but to changes of the hydrogen bond pattern. Since small KIE (< 5) is commonly found when the rate-determining step does not involve H/D exchange,[68] our result is in line with the experimental findings. However, a disparity is noted, in that Kato et al. assumed that the His-mediated mechanism follows an ionic mechanism with the transfer of a proton (through the distal His) and a hydride ion from H_2O_2 to the heme-Cpd I. In contrast, here we have shown that the His-mediated pathway, together with the initial H transfer from H_2O_2 to the oxoferryl (Figure 3), consists, from the electronic point of view, of a hydrogen atom transfer plus a concerted but nonsynchronous electron and proton transfer (H•/ET-H^+).

Direct evidence for the mode in which two protons and two electrons are transferred from the peroxide to catalase Cpd I is not available. Because the distal His is a typical acid−base catalyst, a mechanism in which it delivers a proton from H_2O_2 to the oxoferryl has been proposed, and it has been assumed that the remaining proton plus 2 electrons were transferred directly to the oxoferryl as a hydride ion (the time sequence of these events was not discussed).[13,69] However, hydrogen abstraction or proton coupled electron transfer (PCET) are also compatible with the reaction. Indeed, recent studies on heme enzymes have shown that high valent Fe═O species easily abstract hydrogen atoms or give PCET.[70] Thus, it should not be regarded as surprising that catalase Cpd I undertakes similar elementary steps.

On the contrary, large KIE (10−29) were observed for Leu29His/His64Leu, His64Asp, His64Ala and His64Ser Mb mutants and were ascribed to tunneling effects. In our calculations on catalase, tunneling will likely be at work for the acid−base steps along pathway **A** and the hydrogen transfer process along pathway **B**. However, its effect on the rate of reaction would likely be hidden by the conformational change of the distal His and the hydroxoferryl group, which give higher free energy barriers than the former proton/hydrogen atom transfer events. Results from gas phase calculations on model systems (section 3.4) show that the barrier for the proton transfer increases with increasing interoxygen distance. Thus, the H transfer may turn out to be rate-limiting in case $H_2O_2/HO_2^•$ does not attain short interactions with the oxoferryl/hydroxoferryl unit, resulting in a large KIE. The QM/MM calculations on the His56Gly mutant of HPC suggest that the H-bond network at the distal site plays a key role in positioning the peroxide: in wild-type HPC, the Cpd I:H_2O_2 complex shows a $O-O_a$ distance of 2.60 Å, whereas for the His56Gly *in silico* mutant, it is longer, 2.68 Å, leading to an increased energy barrier for the transfer of H_a. On the other hand, when the distal site cavity is enlarged, as in HPC-His56Gly or in the Leu29His/His64Leu, His64Asp, His64Ala and His64Ser Mb mutants,[14] reorientation of $HO_2^•$ is facilitated and the second Hydrogen transfer easily follows, as has been observed in a nonheme catalase mimic.[34b] Therefore, the initial hydrogen atom transfer, which becomes rate-limiting upon increasing the size of the distal cavity, is likely to be the reason for the large isotope effects found experimentally in certain Mb mutants.

In summary, our calculations show how the kinetics of the reduction of Cpd I by H_2O_2 (a highly exothermic reaction) is modulated by the distal side residues. To facilitate the reaction, a short H-bond has to be attained between the peroxide and the oxoferryl, and after the first H• transfer, either a suitably positioned acid−base catalyst is needed to shuttle a proton to the hydroxoferryl (coupled to an electron transfer), or $HO_2^•$ is allowed to reorient in the distal pocket to transfer the second H atom. Therefore, in line with recent investigations,[15,71] we suggest that Cpd I reactivity depends on the shape and nature of the heme distal pocket. Irrespective of the pathway, the reaction does not proceed through a 2-electron step, as commonly assumed,[2b,3−5] since the two electrons are not transferred simultaneously. Instead, the reaction is better described as two one-electron transfer steps, formally described as H•/ET-H^+ or H•/H•.

Acknowledgment. Dedicated to Professor Santiago Olivella on the occasion of his 65th birthday. This work was supported by Grants 2005SGR-00036 from the *Generalitat de Catalunya (GENCAT)* and FIS2008-03845 from the *Ministerio de Ciencia e Innovación* (MICINN), Spain. Contracts from the Juan de la Cierva program of MICINN (to P.V.) and the F.I. fellowship program of the GENCAT (to M.A.-P.) are acknowledged. We are in debt to Prof. Ignacio Fita for very insightful discussions in the course of this work. We also thank Prof. Peter C. Loewen for a critical reading of this manuscript. We acknowledge the computer support, technical expertise, and assistance provided by the Barcelona Supercomputing Center-Centro Nacional de Supercomputación (BSC−CNS).

Supporting Information Available: Additional computational details, electronic spin distributions along the reaction, system evolution during the metadynamics simulation and potential energy analysis. This material is available free of charge via the Internet at http://pubs.acs.org.

JA9018572

(70) See for instance: (a) Jeong, Y. J.; Kang, Y.; Han, A.-R.; Lee, Y.-M.; Kotani, H.; Fukuzumi, S.; Nam, W. *Angew. Chem. Intl. Engl. Ed.* **2008**, *47*, 7321−7324. (b) Shaik; et al. *J. Am. Chem. Soc.* **2008**, *130*, 10128–10140. (c) Derat, E.; Shaik, S. *J. Am. Chem. Soc.* **2006**, *128*, 13940–13949. (d) Wang, Y.; Chen, H.; Makino, M.; Shiro, Y.; Nagano, S.; Asamizu, S.; Onaka, H.; Shaik, S. *J. Am. Chem. Soc.* **2009**, *131*, 6748–6762.

(71) Poulos, T. L. *J. Biol. Inorg. Chem.* **1996**, *1*, 356–359.